# Well-Controlled Living Polymerization of Perylene-Labeled Polyisoprenes and Their Use in Single-Molecule Imaging

**ARTICLE** *in* MACROMOLECULES · OCTOBER 2006

Impact Factor: 5.8 · DOI: 10.1021/ma0612475



**7 AUTHORS**, INCLUDING:

Robert M Waymouth
Stanford University
**277** PUBLICATIONS **15,608** CITATIONS

SEE PROFILE

William Esco Moerner
Stanford University
**455** PUBLICATIONS **19,597** CITATIONS

SEE PROFILE

# Well-Controlled Living Polymerization of Perylene-Labeled Polyisoprenes and Their Use in Single-Molecule Imaging

**Grant T. Gavranovic,[†] Szilárd Csihony,[‡] Ned B. Bowden,[‡] Craig J. Hawker,[§] Robert M. Waymouth,[‡] W. E. Moerner,*[,‡] and Gerald G. Fuller*[,†]**

*Department of Chemical Engineering, Stanford University, Stanford, California 94305; Department of Chemistry, Stanford University, Stanford, California 94305; and IBM Almaden Research Center, San Jose, California 95120*

*Received June 5, 2006; Revised Manuscript Received September 7, 2006*

ABSTRACT: Functionalized perylene derivatives were synthesized with one or two alkoxyamine units. These compounds were used as initiators in the well-controlled living radical polymerization of isoprene, resulting in polymers with a perylene dye located at either the middle or end of the polymer. Using this approach, polyisoprenes were prepared with similar molecular weights, low polydispersities, and very good initiator efficiencies. Labeled chains were imaged on the single-molecule level in hosts of unlabeled polymer with similar composition. On the time scale from 0.2 to 2−5 s no difference between center- and end-positioned dyes was observed, suggesting that the dynamics outside of this time range should be studied. However, the most rigid host material led to the longest observed correlation times and the highest fraction of fluorophores that exhibited blinking behavior.

## 1. Introduction

The dynamics and rheology of polymer melts are well-studied research topics.[1,2] The rheological character of a material provides important information about the influence of polymer chain architecture on chain orientation, deformation, and relaxation. Various experimental methods, such as forward recoil spectrometry,[3] polarimetry,[4] neutron scattering,[5] and light scattering,[6] have been used to examine the rheology of polymer melts. Recently, single molecules of DNA were observed by labeling the entire chain with multiple fluorescent tags.[7−9] In contrast to this approach, the imaging of single, isolated dye molecules is a technique that allows local heterogeneities in condensed phases to be explored, and it presents several advantages over traditional bulk techniques.[10,11] In this work, dyes are covalently inserted into the polymer backbone to facilitate this sort of single-molecule imaging. The present work is also unique because it is in contrast to previous single-molecule work in polymers, which has generally used free dye molecules as probes of local void and defect environments.[12−16] Specifically, this work uses single, polymer-tethered dye molecules as reporters of the local environments surrounding the center and end positions of polymer chains in the melt.

In previous work from the labs of the authors, several polymers have been prepared with a perylene diimide dye at the end or in the middle of each polymer chain, and the orientation of the labeled segments of polybutadiene (PB) chains in a matrix of poly(methyl methacrylate) (PMMA) was detected using a fluorescence polarization modulation technique.[17] However, the PMMA matrix used in those experiments was glassy, and it is of interest here to study segmental polymer motion in less rigid environments, such as melts and rubbers. To have a close match between the probe molecule and the matrix, it is important that the host polymer and the labeled polymer have nearly the same molecular weight. This can be accomplished with well-controlled living free radical polymerization methods.

Free-radical polymerizations mediated by alkoxyamines were reported recently to control molecule weight accurately, providing low polydispersity.[18] Their functional group tolerance makes alkoxyamines suitable candidates for the synthesis of polymers with predicted length. For studies of the dynamics and rheology of melts, the use of low entanglement molecular weight polymers is also desirable. This allows for the investigation of the molecular dynamics of dyes tethered to highly entangled polymer chains. Polymers made from 1,3-dienes match well with these criteria.[19]

In addition to the syntheses of strategically labeled polyisoprenes (PI), this article will discuss single-molecule measurements of fluorescence emission and dye orientation of these polymer-tethered perylene molecules. Using material previously synthesized[17] as well as new molecules, three host−matrix systems were examined: labeled-PB in PB, labeled-PI in PI, and labeled-PI in a triblock poly(styrene-*b*-isoprene-*b*-styrene) (SIS) rubber. Comparisons of fluorophore dynamics will be made based on location of the dye molecule in the polymer chain backbone, the chemical identity of the dopant and host materials, and the laser illumination intensity. In this preliminary study, only motion over the time window between 0.2 and 2−5 s was explored due to instrumental and material limitations.

## 2. Chemical Synthesis

We report in this paper the well-controlled polymerization of isoprenes and the synthesis of perylene-labeled polymers with the same molecule weight. There are several advantages of the use of isoprene compared to butadiene as simple 1,3-diene precursors. First, isoprene is liquid at room temperature, and it is therefore easier to handle. Also, the polymerization conditions are more controlled and repeatable. Perylene was chosen as the fluorescent tag because of its thermal and photochemical stability, high quantum yield of fluorescence, relative immunity

* Corresponding authors. W.E.M.: e-mail moerner@stanford.edu, phone 650-723-1727, fax 650-725-0259. G.G.F.: e-mail ggf@stanford.edu, phone 650-723-9243, fax 650-725-7294.
[†] Department of Chemical Engineering, Stanford University.
[‡] Department of Chemistry, Stanford University.
[§] IBM Almaden Research Center.

10.1021/ma0612475 CCC: $33.50 
Published on Web 10/19/2006

**Scheme 1. Preparation of Monoalkoxyamine Perylene Diimide**

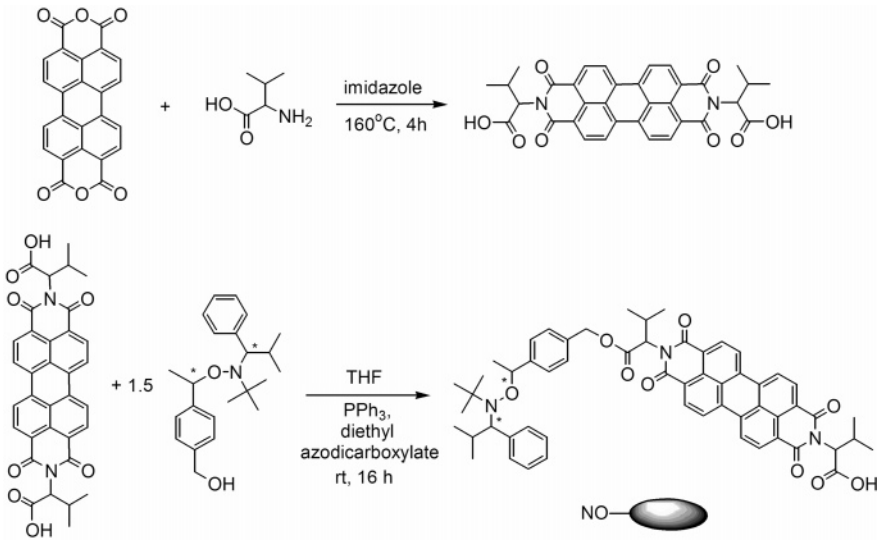


**Scheme 2. Preparation of Dialkoxyamine Perylene Diimide**

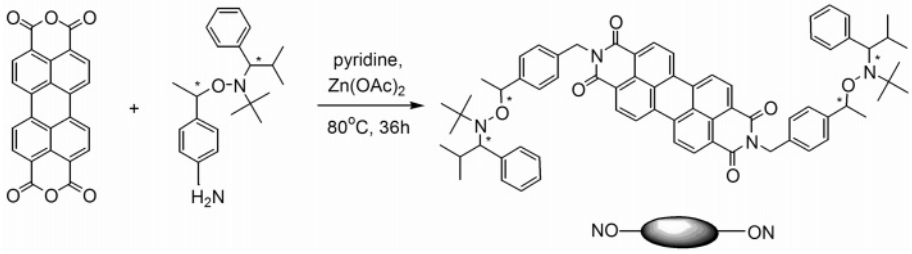


to photobleaching, and easily accessible fluorescence and absorption maxima.[20−22] The initiator alkoxyamine was attached to perylene either directly or through a spacer molecule to produce mono- and disubstituted alkoxyamine perylenes. The synthesis of the monoalkoxyamine derivative was carried out by the condensation of commercially available isoleucine and 3,4,9,10-perylenetetracarboxylic dianhydride followed by esterification with 2,2,5-trimethyl-3-(1′-(4″-hydroxymethyl)phenylethoxy)-4-phenyl-3-azahexane, as illustrated in Scheme 1.

Although this compound was prepared previously,[17] it was only a byproduct in the synthesis of dialkoxyamine perylene. Because esterification can occur at both ends of the perylene, it was reacted with excess alkoxyamine, and the reaction was monitored with TLC. The monoalkoxyamine perylene formed in good yield with this method.

The symmetrically substituted perylene derivative was prepared without amino acid spacer.[23,24] The 3,4,9,10-perylenetetracarboxylic dianhydride was converted efficiently to dialkoxyamine perylene in one step with 1-(4′-aminomethylphenyl)-1-(2″,2″,6″,6″-tetramethyl-1-piperidinyloxy)ethyl,[25] and this process is shown in Scheme 2.

Since the entanglement molecular weight of polyisoprene is ∼5400 g/mol, a molecular weight of 20 000 g/mol was chosen as the target for both labeled and unlabeled polyisoprene synthesis. The isoprene polymerizations carried out are summarized in Table 1. The polymerization experiments were performed at 120 °C in a closed ampule under nitrogen, and the reactions were stopped at low conversion (<40%) to avoid the higher molecular weight shoulder that often forms at higher conversion.[18] It is important that every asymmetrical fluorophore contain one polymer chain and every symmetrical fluorophore contain two polymer chains; thus, for these cases, the efficiency of the initiators must be nearly 100%. The quotient of the weight

**Table 1. Polymerization of Isoprene with Alkoxyamines[a]**

| Entry | Initiator | M/I Ratio | Time (h) | Yield (%) | $M_n$ (g/mol) | PDI | DP | Initiator Efficiency (%) |
|---|---|---|---|---|---|---|---|---|
| 1 | NO | 105 | 20 | 35.2 | 3170 | 1.19 | 41 | 84 |
| 2 | NO | 1440 | 14 | 20.0 | 19500 | 1.17 | 281 | 96 |
| 3 | NO | 960 | 20.5 | 28.9 | 19600 | 1.20 | 282 | 98 |
| 4 | NO | 960 | 24 | 34.4 | 23000 | 1.24 | 332 | 96 |
| 5 | NO—⬭—ON | 1920 | 20.5 | 32.7 | 40700 | 1.53 | 582 | 100 |
| 6 | NO—⬭—ON | 2880 | 6 | 8.6 | 22600 | 1.26 | 316 | 74 |
| 7 | NO—⬭—ON | 2880 | 6.5 | 5.7 | 20200 | 1.24 | 281 | 55 |
| 8 | ⬭—ON | 1440 | 12.5 | 15.1 | 22000 | 1.23 | 309 | 99 |
| 9 | ⬭—ON | 1440 | 14 | 16.1 | 23000 | 1.22 | 324 | 100 |

[a] M/I Ratio = monomer-to-initiator ratio, $M_n$ = number-average molecular weight, PDI = polydispersity index, and DP = degree of polymerization.

of the product and the measured $M_n$ gives the molar amount of the polymer. The initiator efficiency was calculated from the molar ratio of polymer to initiator.

Before the polymerization of isoprenes with the labeled fluorophores was carried out, the basic isoprene polymerization process was optimized with 2,2,5-trimethyl-3-(1-(4-chloromethyl)phenylethoxy)-4-phenyl-3-azahexane. The $^1$H spectra of low-molecular-weight polyisoprene showed the expected signals for both the aliphatic and olefinic protons of the isoprene backbone as well as resonances for the chain ends resulting from the initiating fragments (Table 1, entry 1). This allowed the molecular weight ($M_n$) to be determined from end-group analysis, and the value obtained ($M_n$ = 3090 g/mol) corresponds with that obtained from GPC ($M_n$ = 3170 g/mol). The well-controlled polymerizations of isoprene with $M_n \approx$ 20 000 g/mol with different monomer/initiator (M/I) ratios and reaction times were accomplished with good initiator efficiencies and relatively low polydispersities (Table 1, entries 2−4). Increasing the reaction time gave higher $M_n$ and conversion, which were fully

**Scheme 3. Synthesis of Center-Labeled Polysioprenes**

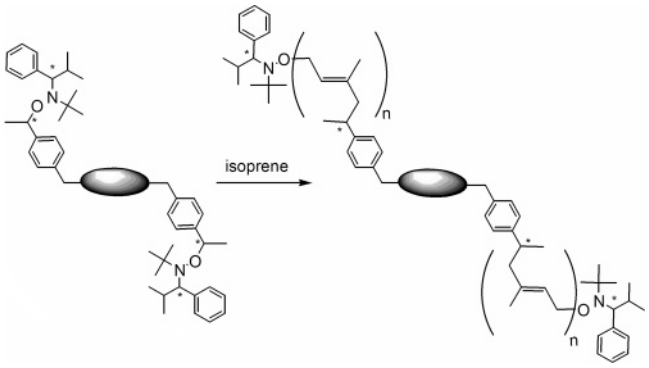


**Scheme 4. Synthesis of End-Labeled Polyisoprenes**

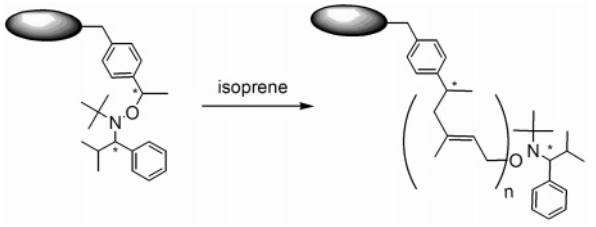


consistent with control experiments and the living mechanism of the polymerization. Although the measurement of high molecular weight polymers is difficult with $^1$H NMR, the difference between the NMR and GPC measured values (DP = 265 and 282, respectively) is within the experimental error of ~10% (Table 1, entry 3).

After the optimization, the polymerization of isoprene was tested with symmetrically substituted perylene initiator, as illustrated in Scheme 3. Polymerization was allowed to proceed until $M_n \approx 20\,000$ g/mol polymer chains were grown onto the each side of the dye. Although the efficiency of the fluorophore initiator was 100% and the target $M_n$ was successfully synthesized, the polydispersity of the polymer was very high (1.53) due to the shoulders in the GPC peak on both higher and lower molecular weight sides (Table 1, entry 5). The preparation of polyisoprene with lower conversion and shorter polymer chains on both sides overcame this problem and gave low, narrow polydispersity polymer (Table 1, entries 6 and 7).

Similar conditions were used in the controlled polymerization of isoprene with monoalkoxyamine perylene and a target molecular weight $M_n \approx 20\,000$ g/mol, and this also produced polyisoprene with low polydispersity and efficient initiator conversion (Table 1, entries 8 and 9). This reaction is shown in Scheme 4. The $M_n$ values calculated from $^1$H NMR for the polymerization with perylene derivatives correspond with those obtained from GPC measurements.

## 3. Single-Molecule Fluorescence Imaging

**3.1. Materials and Methods.** Single-molecule investigations were carried out on perylene-labeled polymers, including those just described. Specifically, poly(butadiene) and poly(isoprene) molecules labeled at either the center or end position were used. Unlabeled matrix polymers were used to dilute the labeled chains so they could be isolated for optical study. In addition to the synthesized materials listed in Table 1, the unlabeled SIS polymer used as a host material for the labeled PI samples was purchased from Scientific Polymer Products (Ontario, NY) and has $M_w = 150\,000$ g/mol and a composition of 14% styrene and 86% isoprene. Triblock SIS is a well-studied system known to form a micellar structure for this composition ratio.[27−29] The center- and end-labeled polybutadienes used here were synthesized by methods described previously,[17] and they had molecular weights of $M_n = 55\,800$ and 43 100 g/mol, respectively.

To prepare samples for single-molecule observation, separate solutions of the labeled and unlabeled polymers were prepared in toluene (Photrex grade, J.T. Baker). The concentration of the labeled polymer was chosen to produce a sample where the fluorophores will be separated by at least the diffraction limit when samples are complete. This generally corresponds to a concentration of $\sim 10^{-10}$ M. The matrix polymer solution had a concentration of 1−5 wt % so that a film with a thickness of about 100 nm will be formed by spin-coating. Film thickness was determined using ellipsometry. To prepare a sample, solutions of the labeled and unlabeled polymers were premixed, and 100 $\mu$L of this mixture was deposited on a plasma-etched no. 1 glass coverslip for spin-coating at 2000 rpm for 30 s. No effort was included to remove oxygen from the samples.

Since cleanliness is of extreme importance in performing single-molecule experiments, all materials were verified to display minimal fluorescent impurities that may interfere with measurements. The unlabeled polymers used as the matrix materials were cleaned by reprecipitation from toluene solution by the addition of methanol. This process was generally repeated three to five times to remove a large fraction of the impurities. Samples made purely from the unlabeled matrix host materials showed two or fewer fluorescent impurities over a 16 $\mu$m$^2$ area. Solvents were also checked for purity, and distillation was used to isolate clean solvent.

The primary components of the fluorescence polarization microscopy apparatus used in these experiments are described here.[30] The light source used was either an $Ar^+$ ion (Coherent Innova) or a semiconductor laser (Novalux Protera) emitting light with a wavelength of 488 nm. This corresponds to a strong absorption peak for perylene diimide. The polarization of the pumping light was modulated using an electrooptic modulator (Conoptics). Using a 495LP dichroic beam splitter, excitation light was directed into an inverted microscope (Nikon Diaphot) equipped with a 100×, NA 1.4, oil immersion objective. Fluorescent light was collected through the objective, and it passed through additional filters to reject undesirable, Rayleigh scattered light. The image was collected using a silicon back-illuminated frame transfer CCD camera (MicroMax, Princeton Instruments). Two phase-locked function generators were used to drive the electrooptic modulator and the camera. The polarization was switched between two orthogonal orientations at a frequency of 5 Hz, and the camera captured images at 10 Hz. This corresponds to one 100 ms frame being recorded during each polarization orientation. With this information, the in-plane dipole orientation angle, $\phi$, can be calculated along with the total emitted intensity, $I_{tot}$. Although the orientation of the molecule with respect to the $z$-axis cannot be determined precisely, changes in $I_{tot}$ may reflect variations in this angle.

**3.2. Results and Discussion.** Several combinations of materials were used for these experiments. In general, it was desired to study labeled polymer chains in a matrix of the same polymer without any label. The specific experiments performed are summarized in Table 2. In all cases, no translational motion was discernible due to entanglement. Labeled-PI was examined in the SIS matrix because the triblock material is 86% isoprene, so its long polyisoprene blocks should appear like a melt to the labeled chains. The labeled-PI in PI systems were studied using a range of laser powers, as measured at the objective, $P_{obj}$, to determine the effect this parameter had on the molecular properties being measured. The laser power can be used to

**Table 2. Summary of the Experimental Systems Examined Using Single-Molecule Fluorescence Microscopy[a]**

| system | no. of molecules | $P_{obj}$ ($\mu$W) | $I_{pump}$ (kW/cm$^2$) | SBR approx |
|---|---|---|---|---|
| center-PB in PB | 279 | 470 | 0.66 | 3 |
| end-PB in PB | 317 | 470 | 0.66 | 8 |
| center-PI in SIS | 113 | 325 | 0.46 | 4 |
| end-PI in SIS | 217 | 325 | 0.46 | 5 |
| center-PI in PI | 479 | 250 | 0.35 | 6 |
| end-PI in PI | 400 | 250 | 0.35 | 5 |
| center-PI in PI | 578 | 500 | 0.71 | 8 |
| end-PI in PI | 427 | 500 | 0.71 | 5 |
| center-PI in PI | 612 | 750 | 1.06 | 4 |
| end-PI in PI | 419 | 750 | 1.06 | 5 |

[a] $P_{obj}$ = laser power at objective, $I_{pump}$ = laser pumping intensity, and SBR = signal-to-background ratio.

determine the pumping intensity, $I_{pump}$, by using the characteristic size of the laser beam at the sample. Furthermore, the signal-to-background ratio (SBR) for each case is presented, indicating that single molecules can be clearly observed. As Table 2 illustrates, the experiments performed allow for the analysis of the importance of three primary factors: position of the dye molecule in the chain, chemical identity of the dopant and matrix polymers, and pumping intensity.

Four consecutive frames from one of these experiments are shown in Figure 1. The signal for each fluorophore is clearly distinguishable from nearby molecules and from the background. For a typical sample, data can be collected for up to 60 s, by which point the fluorophores in view have almost entirely ceased emission by photobleaching. The intensity profile for a single molecule can be recorded as a function of time, and the recorded intensities corresponding to each polarization compose a time-trace plot when the camera offset and background are subtracted. For each consecutive pair of intensities, one with each polarization, an azimuthal orientation angle can be calculated from the expression

$$\phi = \frac{1}{2}\cos^{-1}\left(\frac{1 - I_y/I_x}{1 + I_y/I_x}\right) \quad (1)$$

Thus, $\phi$ values can only be determined every 200 ms. The orientation angle is only of interest when the molecule is fluorescing.

**3.2.1. Characteristic Behavior.** The fluorophores observed here showed behavior typical of single molecules. Most clearly, the vast majority of dyes exhibited digital on−off transitions, and those that did not were not included in the analysis. As was reported by Bowden et al., we also observe a variety of characteristic dye behaviors.[17] Some dyes are essentially locked in one position over the course of an experiment, while others demonstrate either smooth or discrete reorientation. Many of the molecules demonstrate blinking—an on−off−on transition—and the orientation of the dye may either change or stay the same during this process as well. Time trace plots and angle−intensity plots are presented here to show some of the typical behaviors observed for these polymer-tethered dye molecules. No observed behaviors were unique to any particular experimental system.

Figure 2 depicts a molecule whose orientation is essentially fixed over the course of its lifetime. It happens that this dye is almost aligned with the axis defined by *x*-polarized excitation light, so the $\phi$ values are less than 30°. Figure 3 depicts a molecule that blinks and appears to be in a different orientation during its second on-time. In this case, the total intensity during the second on-time is larger than during the first. This could correspond to a realignment of the molecule into the plane normal to the laser propagation axis. Additionally, when a molecule is oriented more out of plane, the projections of its transition dipole moment on the two orthogonal axes in the plane normal to the laser axis are more equally distributed, giving nearly equal contributions in the *x*- and *y*-channels before the dark state is observed. There is a small amount of variance in the calculated angle that arises from the finite number of photons detected; however, the standard deviation in most cases, including those shown in these figures, is ~1.3°.

**3.2.2. Autocorrelation Function Analysis.** As the preceding plots demonstrate, we are able to observe fluctuations in both the emitted intensity and the orientation of these polymer-tethered dyes on the single-molecule level in real time. To quantify these behaviors, autocorrelation function (ACF) analysis was used for both the total projected intensity and the azimuthal orientation angle, determined using eq 1, as functions of time. However, on the time scale between 0.2 s (the acquisition time) and 2−5 s (the typical photobleaching time), the subtle differences between the end- and center-attached dyes cannot be easily observed using our approach. The most readily apparent variations in behavior were due to changes in the matrix material surrounding the labeled polymers.

Once the autocorrelation functions had been generated, the statistically significant portions of the curves were fit to a single-exponential decay. This analysis included only points outside the confidence limits arising from finite trajectory length and excluded the point at zero lag due to the large contribution from pure noise.[31] A sample ACF curve with the confidence limit and the exponential decay fit is shown in Figure 4. While the single exponential fit is adequate, it does not capture the shape of every distribution. An alternate approach would be to simply define the relaxation time as the time necessary for the ACF value to reach 1/*e* of its original value. As this plot shows, the confidence limit can significantly reduce the number of valid data points. This is particularly limiting for data sets with small numbers of points, as was often the case in analyzing the orientation angles in this work. These angles were only studied during the fluorescence process, and these periods often lasted only a few seconds.

The primary piece of information the ACF analysis provides is the correlation decay time that characterizes the exponential

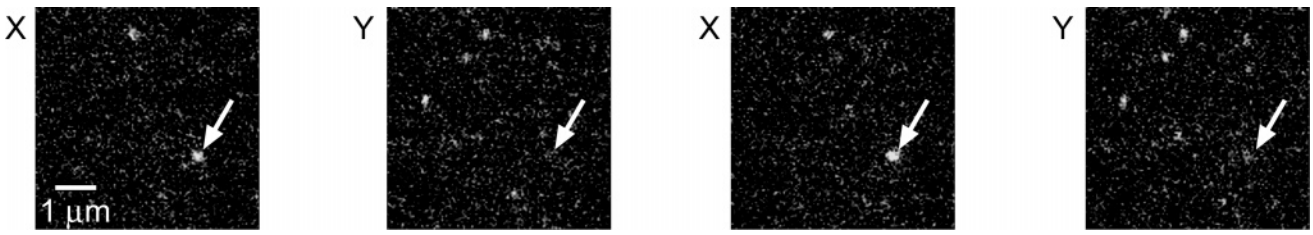


**Figure 1.** Sample images of polymer-tethered perylene molecules taken using the polarization-modulated epifluorescence configuration described in the text. These are consecutive images, separated by 100 ms and illuminated with light of two orthogonal polarizations in the $X-Y$ plane. The arrow indicates a molecule that is excited by only one polarization due to its orientation.

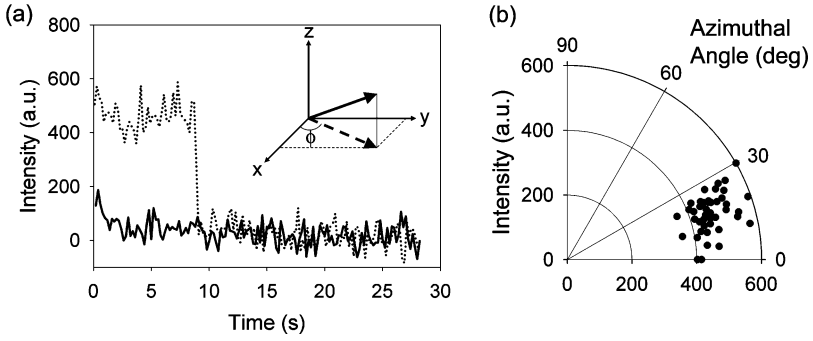


**Figure 2.** A molecule whose orientation is essentially fixed. (a) $I_x$ (···) and $I_y$ (—) as functions of time. (b) Corresponding in-plane orientation angle, $\phi$, of this molecule during the time it is emitting light. These figures are for a center-labeled PB chain in PB. Inset: experimental reference frame showing $\phi$ relative to the two polarization axes, $x$ and $y$, and the laser propagation axis, $z$.

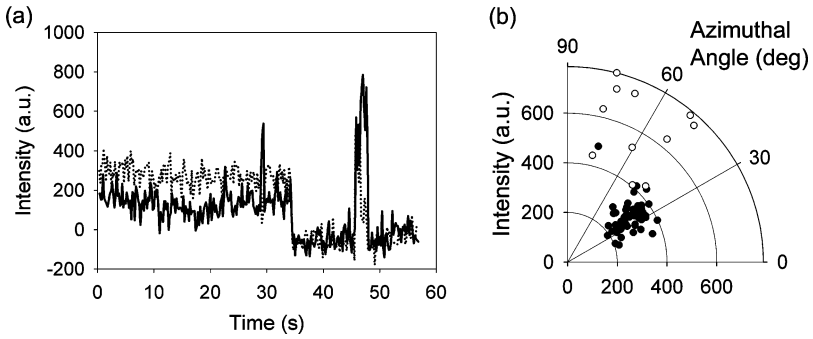


**Figure 3.** A molecule that blinks and changes orientation. (a) $I_x$ (···) and $I_y$ (—) as functions of time. (b) Corresponding in-plane orientation angle, $\phi$, of this molecule during the first (●) and second (○) on-times. These figures are for a center-labeled PB chain in PB.

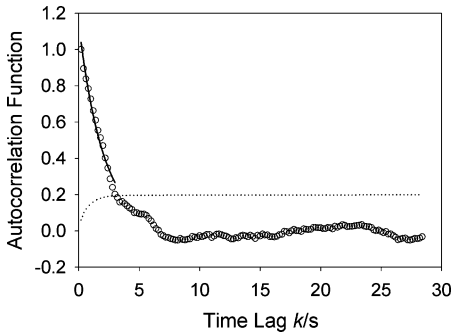


**Figure 4.** A sample plot of an autocorrelation function as a function of lag time. The confidence limit, defined by the standard error, is also included (···). A single-exponential fit is shown for the statistically significant points (—). This figure presents the ACF of the total emitted intensity for a center-labeled PI chain in PI, and the exponential decay fit has a decay time of 1.9 ± 0.05 s.

fit to the valid data points. The decay times for different molecules can then be collected into a histogram so the full distribution of behaviors can be examined. These histograms reflect the heterogeneity of the polymer system. In most cases studied here, these histograms could also be fit with a single-exponential curve, yielding another characteristic time which describes the typical response across all molecules in that population. However, there is no particular model that predicts an exponential distribution of decay times. The observed distributions may be the long-time tail of a distribution peaking at times shorter than can be measured with the current setup.

The ACF values for the total projected fluorescence intensity were calculated based on the entire period of data collection, and they should reflect the effects of all fluctuations in intensity. This includes small contributions, such as the molecule rotating into or out of the plane of the stage, as well as large contributions, such as the transition from emitting to being dark. The length of time a molecule is in each phase—either on or off—will be reflected in the autocorrelation function.

The intensity ACFs were calculated for all the molecules studied, and the results for the characteristic decay times are discussed here in an effort to elucidate the effects of the three parameters being tested: dye position, material identity, and illumination power. To address the importance of the position of the dye along the chain, the data were grouped so that the results for center-labeled chains, for example, reflect experiments on center-PB in PB, center-PI in SIS, and center-PI in PI. Using this approach, the histograms of the intensity ACF decay times for all center- and end-labeled polymer chains were studied. However, these data suggest no discernible difference in the correlation times for center-positioned dyes relative to end-positioned dyes.

Figure 5 includes intensity ACF decay time distributions comparing the different materials studied. Specifically, data are summed across both dye locations to isolate the effect of the dopant−host system. The labeled-PI in SIS system shows a distribution weighted toward longer correlation times, and the labeled-PI in PI system displays the shortest decay times of the three systems. The viscosities of these systems may play a role in these observations. Since it is a physically cross-linked rubber, the SIS matrix is the most rigid environment. While the other two matrices are polymer melts, the unlabeled-PB used has a higher molecular weight than the PI. In fact, the viscosity of the PB matrix is expected to be ∼10 times greater than that of PI. If the rigidity of the local environment plays a significant role in affecting the photophysical behavior, such as by hindering bending or rotation of the dye molecule, this may explain the observed results.

The effect of laser illumination power on the intensity autocorrelation functions was also examined using the same

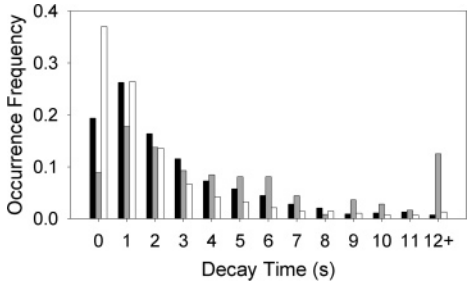


**Figure 5.** Histograms comparing the intensity ACF decay times for labeled-PB in PB (black), labeled-PI in SIS (gray), and labeled-PI in PI (white). Because of the shapes of the distributions, the standard single-exponential decay analysis could not be used here. Inspection of the histograms suggests that dyes in the SIS host show the longest correlation times, while those in the PI host have the shortest. In this histogram, the numbers of molecules studied are $N_{PB^*-PB} = 537$, $N_{PI^*-SIS} = 248$, and $N_{PI^*-PI} = 2758$.

approach; however, the data do not suggest a uniform trend in the ACF decay times as illumination intensity is varied.

In addition to the intensity ACFs, autocorrelation function analysis was also performed on the azimuthal orientation angle as a function of time. Results from the angle ACFs should primarily reveal information about the rate at which the dyes reorient in the sample; however, there is also a contribution from intensity fluctuations that affects the calculation of the orientation angle. The same cases analyzed for the intensity ACFs were also studied using the angle ACFs. A notable difference is that the orientation angles were only studied while the molecules were emitting light, while the intensity ACFs were based on the entire period of data collected. A significant consequence of this difference is that the angle ACFs are based on many fewer data points, and this results in the confidence limits being more restrictive, which further reduces the number of usable ACF points. It should also be noted that many angle ACF curves appear to show decaying oscillatory behavior; however, because the magnitude of this fluctuation falls inside the prescribed confidence limits, nothing concrete can be concluded. Previous observations of oscillatory ACFs have been reported and attributed to dye rotation.[14]

As was the case with the intensity ACFs, the histograms of the angle ACF decay times for center- and end-tethered dyes also show correlation times that are indistinguishable. Since the observed histograms are not drastically different from one another, a consideration is that the dye molecules themselves are playing a large role in determining their orientations instead of reflecting the motion of the polymers to which they are attached. A final possibility is that the fluctuations arising from polymer segmental motion lie at time scales faster than the 200 ms time resolution of this experiment. This could be explored by faster recording of the emitted photons.

The results of the angle ACF analysis for the labeled polymers in each host again lead to conclusions are similar to those from the intensity ACF calculations. Molecules in the SIS host show the longest decay times, and this may be due to the rigid structure of the matrix material.

The angle ACF results highlighting the effect of changing the illumination intensity were also studied. Interestingly, these data do not reflect the same conclusions as the intensity ACF analysis. Here, increasing the illumination intensity leads to a shift to shorter correlation times, while no trend was apparent in the intensity ACF results. This seems to suggest that higher laser powers do make the dye molecules reorient more quickly, but they do not lead to observable changes in blinking frequency and on-time length.

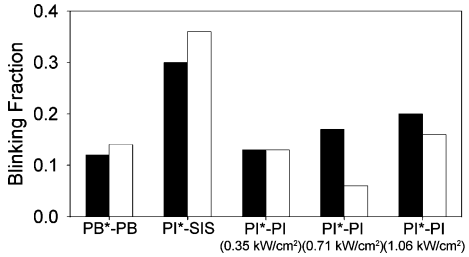


**Figure 6.** Bar graph comparing the fractions of molecules that blink during the course of observation for each experimental system. In general, there are no clear trends between center- (black) and end-labeled (white) chains or as a function of illumination intensity. However, a higher fraction of the dyes in the SIS host blink compared to any of the other systems.

Blinking is another aspect of the observed behavior that was analyzed. As mentioned previously, the causes of single-molecule blinking are still not well understood, but further observations of when it occurs may make its origins more clear. Figure 6 compares the fractions of the observed molecules that blink at some point during the observed period for each experimental system. Neither the position of the dye at either the center or end position nor the illumination intensity seems to affect the blinking behavior. However, the host material does seem to play a role, as the dyes in the SIS matrix blink more frequently than either of the other dopant−host combinations. It is interesting to note that even though these dyes in SIS display the highest fraction of molecules that blink, they also display the longest correlation times based on the intensity ACF analysis, as shown in Figure 5. Therefore, even though many of the molecule blink, they still spend the longest times in each on- or off-state compared to the other systems studied.

## 4. Conclusions

In this work, we report the well-controlled living radical polymerization of polyisoprene, and the application of this method to synthesize polymers with single perylene molecules built into the backbone at either the center or end position. We have also used polarization-modulated fluorescence microscopy to study these labeled polymers on the single-molecule level. This allows the observation of emitted intensity corresponding to excitation with each of two orthogonal polarizations, and this information can be used to determine the projected orientation of the dye and an in-plane azimuthal angle describing its position. In all cases, the use of a single-molecule level approach allowed a variety of behaviors to be of observed, and this heterogeneity reflects the unique properties of each molecule in response to its local environment. To reiterate, the behavior histograms were fit with single-exponential curves to allow for convenient comparison between different populations; however, the fact that the histogram looks "exponential" should not be regarded as fundamental or expected.

Using autocorrelation analysis of both the total emitted intensity and the orientation angle, a few conclusions were reached. First, there is no distinguishable difference in the characteristic correlation times between center- and end-positioned dyes. Also, molecules in the rubbery SIS matrix display the longest correlation times, while those in the low-viscosity PI host display the shortest times. Finally, the laser illumination intensity had little impact on the intensity ACF decay times, but higher intensity did lead to shorter correlation times in the angle ACF analysis. This seems to suggest that high intensity provides more thermal energy for the molecules to reorient, but it does not significantly affect the length of time the dyes spend in on- or off-states.

The blinking behavior of these dyes was also analyzed, and while neither dye position nor laser power contributed significantly to the fraction of molecules that blinked, the choice of matrix material has a large impact. Again, the SIS host stood out; this time because dyes in this material displayed a blinking fraction approximately twice as large as any other system.

There are several experimental concerns that should be kept in mind. The dye molecule is quite large compared to the size of a monomer, so the innate motion of the chain may be altered. Thus, while the observed motion of the dye molecules in this work may not be representative of unhindered polymer motion, these dyes certainly behave as reporters of the local environment surrounding their position at either the chain end or the chain center. This is in contrast to previous studies where free single-molecule chromophores have been doped into polymer hosts and no control over the dye location is possible. The similar behaviors for end- and center-labeled dyes in the present work might then suggest that there is, by this technique, no observable difference in the local environments in the vicinity of chain ends vis-à-vis chain centers. Further experiments could be performed to examine untethered fluorophores in these polymer melts to compare their behavior to those built into the polymer backbone. Second, the films used here were ~100 nm thick to maintain focus and minimize background signal. This thinness results in a large amount of surface area, both in contact with the glass substrate and exposed to air. This could allow for a fraction of the dyes being studied to become stuck on the glass or experience chemical reactions with oxygen that may change their photophysical properties. Additionally, the dynamic properties of the polymer film itself will be different near each of these interfaces. Finally, in contrast to previous work performed using glassy polymer hosts, the dyes in these melts displayed shorter times of emission before photobleaching. Often, molecules would only emit light for less than 1 s. These short emission periods made data analysis difficult since statistical error was often limiting. It seems that the increased mobility of the host material or the increased permeability to oxygen may contribute to limiting this lifetime. Working under an inert environment or using time-lapse imaging may allow for the study of behavior on longer time scales. Additionally, improved detectors are now available that might allow for the use of lower illumination intensities, which can also lead to longer emission times. To examine shorter time scales, time-tagging of the emitted photons may be beneficial. By using approaches such as these, a wider range of time scales could be explored.

**Acknowledgment.** The authors acknowledge support from NSF-DMR-0237247 and the Center on Polymer Interfaces and Macromolecular Assemblies (NSF-DMR-0213618). Also, Dr. Katherine Willets made significant contributions in a number of areas, including training, apparatus setup, and experimental advice.

## References and Notes

(1) Larson, R. G. *The Structure and Rheology of Complex Fluids*; Oxford University Press: New York, 1999.
(2) Macosko, C. W. *Rheology: Principles, Measurements, and Applications*; VCH Publishers: New York, 1994.
(3) Shull, K. R.; Dai, K. H.; Kramer, E. J.; Fetters, L. J.; Antonietti, M.; Sillescu, H. *Macromolecules* **1991**, *24*, 505.
(4) Fuller, G. G. *Optical Rheometry of Complex Fluids*; Oxford University Press: New York, 1995.
(5) Higgins, J. S.; Benoit, H. C. *Polymers and Neutron Scattering*; Clarendon Press: Oxford, 1994.
(6) Lodge, T. P. *Macromolecules* **1983**, *16*, 1393.
(7) Perkins, T. T.; Smith, D. E.; Chu, S. *Science* **1994**, *264*, 819.
(8) Perkins, T. T.; Quake, S. R.; Smith, D. E.; Chu, S. *Science* **1994**, *264*, 822.
(9) Perkins, T. T.; Smith, D. E.; Chu, S. *Science* **1997**, *276*, 2016.
(10) Moerner, W. E.; Kador, L. *Phys. Rev. Lett.* **1989**, *62*, 2535.
(11) Moerner, W. E.; Fromm, D. P. *Rev. Sci. Instrum.* **2003**, *74*, 3597.
(12) Hou, Y.; Bardo, A. M.; Martinez, C.; Higgins, D. A. *J. Phys. Chem. B* **2000**, *104*, 212.
(13) Bartko, A. P.; Dickson, R. M. *J. Phys. Chem. B* **1999**, *103*, 3053.
(14) Bartko, A. P.; Xu, K.; Dickson, R. M. *Phys. Rev. Lett.* **2002**, *89*, 026101.
(15) Weston, K. D.; Goldner, L. S. *J. Phys. Chem.* **2001**, *105*, 3453.
(16) Tomczak, N.; Vallé, R. A. L.; van Dijk, E. M. H. P.; Garc×c1a-Parajó, M.; Kuipers, L.; van Hulst, N. F.; Vancso, G. J. *Eur. Polym. J.* **2004**, *40*, 1001.
(17) Bowden, N. B.; Willets, K. A.; Moerner, W. E.; Waymouth, R. M. *Macromolecules* **2002**, *35*, 8122.
(18) Benoit, D.; Harth, E.; Fox, P.; Waymouth, R. M.; Hawker, C. J. *Macromolecules* **2000**, *33*, 363.
(19) Fetters, L. J.; Lohse, D. J.; Milner, S. T. *Macromolecules* **1999**, *32*, 6847.
(20) Langhals, H.; Demmig, S.; Potrawa, T. *J. Prakt. Chem./Chem.-Ztg.* **1991**, *333*, 733.
(21) Langhals, H. *Heterocycles* **1995**, *40*, 477.
(22) O'Neil, M. P.; Niemczyk, M. P.; Svec, W. A.; Gosztola, D.; Gaines, G. L., III; Waskelewski, M. R. *Science* **1992**, *257*, 63.
(23) Rohr, U.; Schlichting, P.; Böhm, A.; Gross, M.; Meerholz, K.; Bräuchle, C.; Müllen, K. *Angew. Chem., Int. Ed.* **1998**, *37*, 1434.
(24) Würthner, F.; Thalacker, C.; Sautter, A.; Schärtl, W.; Ibach, W.; Hollricher, O. *Chem.—Eur. J.* **2000**, *6*, 3871.
(25) Dao, J.; Benoit, D.; Hawker, C. J. *J. Polym. Sci., Part A* **1998**, *36*, 2161.
(26) Benoit, D.; Chaplinski, V.; Braslau, R.; Hawker, C. J. *J. Am. Chem. Soc.* **1999**, *121*, 3904.
(27) Hotta, A.; Clarke, S. M.; Terentjev, E. M. *Macromolecules* **2002**, *35*, 271.
(28) Kim, J. K.; Lee, H. H.; Gu, Q.-J.; Chang, T.; Jeong, Y. H. *Macromolecules* **1998**, *31*, 4045.
(29) Adams, J. L.; Graessley, W. W.; Register, R. A. *Macromolecules* **1994**, *27*, 6026.
(30) Willets, K. A. Doctoral Thesis, Stanford University, Stanford, CA, 2005.
(31) Box, G. E. P.; Jenkins, G. M. *Time Series Analysis: Forecasting and Control*, Rev. Ed.; Holden-Day: San Francisco, 1976.

MA0612475